24th COBEM - 2017

24th ABCM International Congress of Mechanical Engineering
December 3-8, 2017, Curitiba, PR, Brazil

COBEM-2017-1000
EVALUATION OF TEXTURING EFFECTS ON HYDRODYNAMIC BEHAVIOR OF JOURNAL BEARINGS

Leandro Ito Ramos
Gregory Bregion Daniel
State University of Campinas – School of Mechanical Engineering
leandroito@fem.unicamp.br, gbdaniel@fem.unicamp.br

Abstract. *This work evaluates texturing effects on the hydrodynamic behavior of journal bearings by analyzing the load carrying capacity and power loss. The classical Reynolds equation is considered as lubrication model and the Finite Volume Method (FVM) is used to evaluate the problem. A Full Multigrid (FMG) algorithm is employed to solve in a fast way these discrete equations. Partial and full texturing are studied, varying the operating conditions, and best textures parameters for each case are evaluated through Design of Experiments (DOE). Results show that power loss on journal bearing can be reduced with the proper choice of textures radius and maximum local depth, which strongly depends on operating conditions.*

Keywords: *journal bearing, hydrodynamic lubrication, surface textures, FVM, FMG*

1. INTRODUCTION

Journal bearings are applied in rotating machinery in order to guarantee a relative motion between the shaft/rotor and the supporting structure. Main purpose of this component is to provide load carrying capacity through the thin oil film being moved along with the shaft inside the journal bearing. The shaft's lift characterizes a hydrodynamic lubrication condition inside the journal bearing, dramatically reducing the power loss inside that machine element. Several attempts were made in order to improve its performance mostly by modifying journal bearings' geometry, but recently tribological approaches have been explored to achieve the desired optimization (Etsion, 2013; Wang, 2014; Gropper et al, 2016). In this case, the changes consist on the introduction of textures distributed over some specific areas of journal bearing's inner surface (partial texturing) or its entire area (full texturing).

Optimization of journal bearing's main operating parameters is an important topic of research once its development should follows the accelerated rhythm with which rotating machineries and its components are innovated. Journal bearings have a great influence over dynamic and static behaviors of rotating machines and therefore should not be neglected while the rest of the assembly is developed. For instance, the insertion of textures on component's surface could improve lifting on the journal bearing while reducing the amount of energy lost during its operation by the viscous forces. The oil starvation's probability of occurrence could also be reduced since textures can act as lubricant reservoirs. However, an extensive study must be done in order to choose the best surface texture's parameters and distributions.

At the same time, a tribological approach turns the problem into a multiscale analysis from a numerical perspective and therefore a fast and efficient solver must be used for solving the discrete system of equations. For this purpose, a Full Multigrid Algorithm (FMG) is employed in this study.

The first part of this paper presents a description of the lubrication phenomena occurring on a journal bearing, through the Reynolds equation, and the modifications needed on oil film thickness equation when texturing its surface. Next are discussed the discrete formulation of the problem obtained through the Finite Volume Method (FVM) and the multilevel technique used to solve it. Then the main part of the study is exposed, in which consists of the analysis of surface texturing's effects on journal bearings static characteristics, i.e. load-carrying capacity and viscous shear force, in order to determine the best choice for textures radius and maximum local depth, while considering two different equilibrium positions (shaft eccentricity) of the machine component.

2. METHODOLOGY

Figure 1 shows a schematic representation of a journal bearing. As can be seen in Fig. 1(a), e is the shaft's eccentricity which has two Cartesian components $e_x = e\sin(\phi)$ and $e_y = -e\cos(\phi)$, where ϕ is the attitude's angle. Thus, the pair (e,ϕ) indicates shaft's position relative to the bearing in polar coordinates. In Fig. 1(b) a journal bearing planned view is shown exemplifying textures distribution, which follows the pattern used by Tala-Ighil and Fillon (2011).

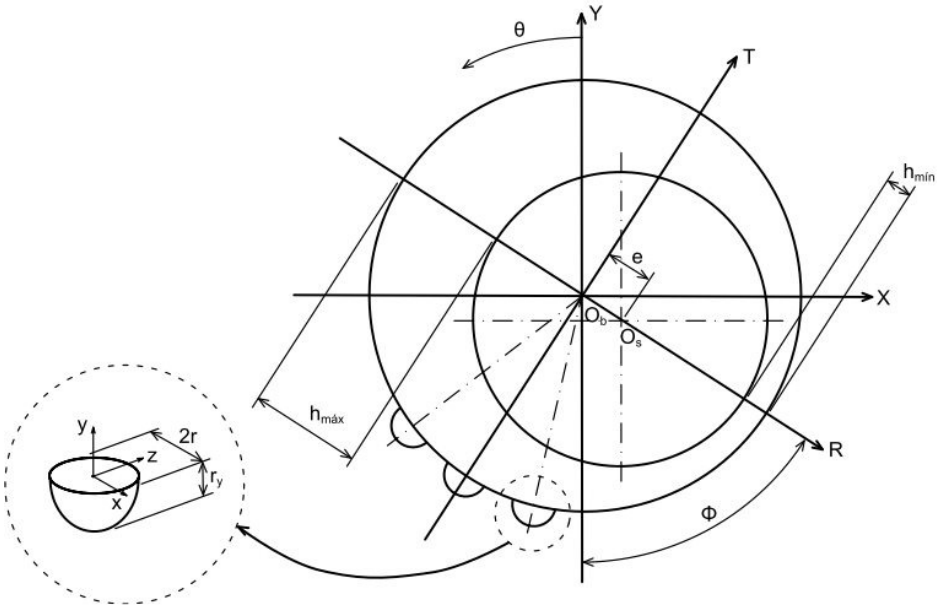

(a)

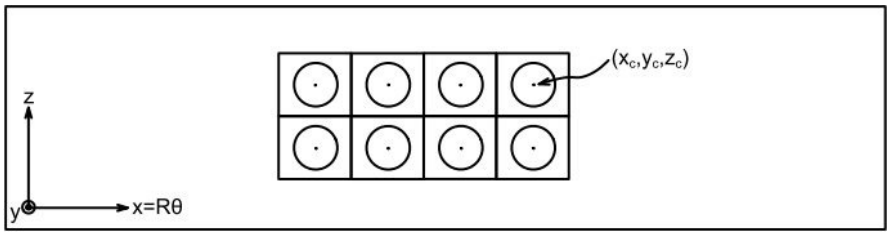

(b)

Figure 1. Scheme of a textured journal bearing

2.1 Reynolds equation in cartesian coordinates and surface texturing

Once the shaft starts to rotate inside the journal bearing the oil film's pressure distribution is generated. This generated pressure field can be mathematically described through the classical Reynolds equation, written for the static condition and on Cartesian coordinates as follows:

$$\frac{\partial}{\partial x}\left(h^3\frac{\partial p}{\partial x}\right)+\frac{\partial}{\partial z}\left(h^3\frac{\partial p}{\partial z}\right)=6\mu\omega R\frac{\partial h}{\partial x} \tag{1}$$

where p is the pressure on the lubricant film, μ is the lubricant's dynamic viscosity, ω the shaft's rotational speed and R is the shaft's radius. The lubricant film thickness h for a smooth journal bearing can be defined as:

$$h(\theta) = C_r + e_x\sin(\theta) - e_y\cos(\theta) \tag{2}$$

in this case C_r is the journal bearing's radial clearance and θ the angular coordinate established on the inertial coordinate system XY from Fig. 1(a). The choice for an inertial coordinate system aims to ease the way surface textures can be distributed in this reference system in terms of coding.

The introduction of textures, which can also be called by dimples, on the journal bearing surface includes a correction term on Eq. (2), as follows:

$$h(\theta, z) = h(\theta) + \Delta h(\theta, z) \tag{3}$$

where the correction term Δh is the dimple's local depth. For this study, a spherical cap geometry for the textures was adopted and therefore Δh is given by the following relation from Tala-Ighil and Fillon (2011):

$$\begin{aligned} &\Delta h(\theta, z) = \frac{r_y}{r}\sqrt{r^2 - (x - x_c)^2 - (z - z_c)^2} \quad \text{when } \sqrt{(x - x_c)^2 + (z - z_c)^2} \leq r \\ &\Delta h(\theta, z) = 0 \qquad\qquad\qquad\qquad\qquad\qquad\qquad\qquad\quad \text{otherwise} \end{aligned} \tag{4}$$

where r_y and r are, respectively, the height of the spherical cap and the radius of the circle on the bearing's surface according to Fig. 1. The center of a texture on bearing's surface is given by the coordinates (x_c, y_c, z_c), where $y_c = 0$, as shown in Fig. 1. In this study, textures are distributed as shown in Fig. 2 and Reynolds cavitation condition was adopted for Eq. (1).

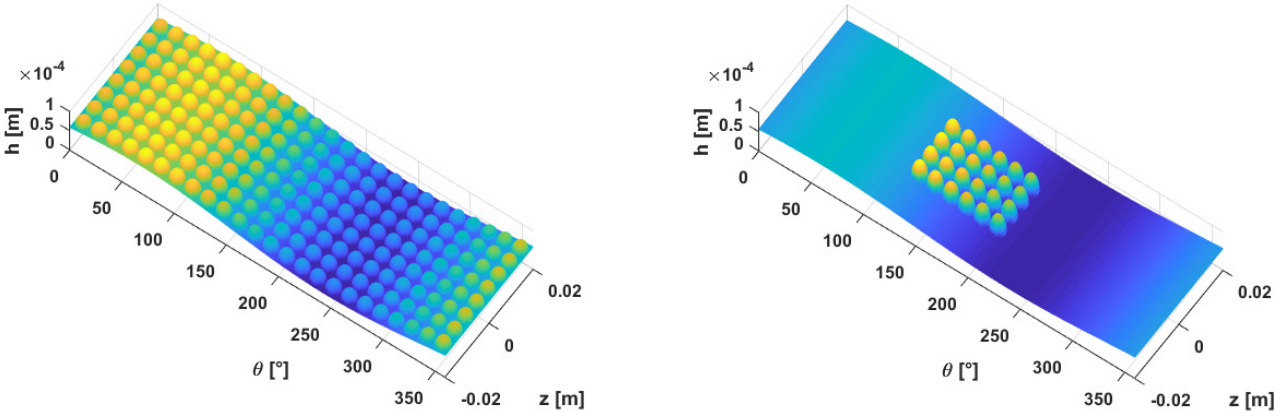

(a) (b)

Figure 2. Two examples of lubricant film thickness distribution exemplifying studied surface textures distributions; (a) full textured journal bearing; (b) partial textured journal bearing.

2.2 Discrete problem formulation and solution with multilevel technique

As previously mentioned, the FVM is applied to solve numerically the classical Reynolds equation. The partial derivatives that describe the pressure gradient in the boundaries of the volumes are approximated by the central differences scheme. Thus, the integration of the Reynolds equation leads the linear equation presented as:

$$C_P p_P = C_N p_N + C_S p_S + C_E p_E + C_W p_W + B \tag{5}$$

with

$$C_{E,W} = \frac{\Delta z}{\Delta x} h_{e,w}^3 \tag{6}$$

$$C_{N,S} = \frac{\Delta x}{\Delta z} h_{n,s}^3 \tag{7}$$

$$C_P = C_N + C_S + C_E + C_W \tag{8}$$

$$B = 6\mu\omega R\Delta z(h_w - h_e) \tag{9}$$

where C are pressure's coefficients, B is the source term, Δx and Δz are, respectively, volume's size in x and z directions. Sub index in Eqs. (5) - (9) means the cardinal orientations used in the computational mesh.

As the FVM mesh is refined the number of linear equations given by Eq. (5) grows accordingly. Shaft equilibrium position inside the journal bearing allows to evaluate its load-carrying capacity and power loss, but if a non-efficient solver for the pressure distribution's discrete problem is adopted a lot of computer time is consumed even using the efficient search algorithm of Newton-Raphson for that equilibrium position. In that sense, the implementation and use of an efficient solver such as FMG should not only down grade computational cost but allow the use of more refined meshes and therefore reduce discretization error. In order to solve quickly the discrete problem, a FMG algorithm was implemented following the proposed algorithm from Venner and Lubrecht (2000).

2.3 Journal bearings static characteristics

Once the pressure field inside journal bearing is obtained the hydrodynamic forces are calculated as follows:

$$F_y = \sum_i \sum_j p_{i,j} \cos(\theta)\Delta x\Delta z \tag{10}$$

$$F_x = \sum_i \sum_j p_{i,j} \sin(\theta)\Delta x\Delta z \tag{11}$$

and the shaft's equilibrium condition is achieved when $F_y = W$ and $F_x = 0$, with W the loading acting vertically on the shaft. Moreover, the viscous shear force can be calculated in order to observe power losses due to viscous friction inside lubricant film as follows:

$$F_s = \sum_i \sum_j \left(\mu \frac{\omega R}{h_{cv_{i,j}}} + \frac{h_{cv_{i,j}}}{2} \frac{\Delta p}{\Delta x} \right) \Delta x\Delta z \tag{12}$$

with $h_{cv_{i,j}}$ the oil film thickness at the (i^{th}, j^{th}) volume's center from the FVM mesh and the pressure gradient $\frac{\Delta p}{\Delta x}$ is calculated using the central differences scheme.

3. RESULTS AND DISCUSSIONS

3.1 Simulation Parameters and Experimental Tree

Journal bearings operating conditions and geometrical parameters were adopted from Kango (2014). A FVM mesh with $N_x = 580$ x $N_z = 184$ was used to achieve a satisfactory low discretization error and properly detect surface textures even on FMG coarser grids. The multilevel technique was settled to work with 4 levels and a number of pre and post-relaxations equal to 8 and 4, respectively. Relative tolerances for multilevel correction cycle and its inner Gauss-Seidel method were settled by 10^{-3} and 10^{-7}, respectively.

The observed journal bearing's static characteristics are shaft's equilibrium position, given by e and ϕ, and the resultant viscous shear force F_s. The first allows to easily see whether load-carrying capacity is diminishing or growing up with surface textures insertion on the journal bearing. The second is directly related to power losses on journal bearing.

Table 1 shows the experimental tree and corresponding simulation results, where $\varepsilon = \frac{e}{C_r}$ is the eccentricity ratio. Experimental tree was structured such that for each specific journal bearings' operating conditions and textured portion were evaluated the effects of surface textures' radius and maximum local depth, including their possible interactions,

over the chosen responses. The percentage deviations are relative to the respective smooth bearings parameters and are used in the subsequent analysis.

Table 1. Simulation results

ω $[rpm]$	W $[N]$	*texturing*	r $[mm]$	r_y $[\mu m]$	ε	F_s $[N]$	ε (%)	F_s (%)
1500	1350	*full*	1.25	20	0.3422	26.7422	12.34	–1.38
1500	1350	*full*	1.25	40	0.3685	26.8533	20.98	–0.98
1500	1350	*full*	2.25	20	0.4305	25.6069	41.33	–5.57
1500	1350	*full*	2.25	40	0.5283	26.0592	73.44	–3.90
1500	1350	*partial*	1.25	20	0.2984	26.9717	–2.04	–0.54
1500	1350	*partial*	1.25	40	0.2974	26.9473	–2.36	–0.63
1500	1350	*partial*	2.25	20	0.2832	26.5995	–7.03	–1.91
1500	1350	*partial*	2.25	40	0.2780	26.4728	–8.73	–2.38
1500	6600	*full*	1.25	20	0.7402	40.7012	5.49	2.52
1500	6600	*full*	1.25	40	0.7660	42.0441	9.16	5.90
1500	6600	*full*	2.25	20	0.8251	42.6354	17.59	7.39
1500	6600	*full*	2.25	40	0.8558	43.5457	21.96	9.69
1500	6600	*partial*	1.25	20	0.7018	39.5855	0.01	–0.29
1500	6600	*partial*	1.25	40	0.7081	39.9240	0.91	0.56
1500	6600	*partial*	2.25	20	0.6978	39.0503	–0.56	–1.64
1500	6600	*partial*	2.25	40	0.7138	39.9136	1.72	0.54

Results shown in Tab. 1 are analyzed in the following sections. First the viscous shear force is analyzed as response exploring a portion of the project domain and analyzing best tendencies for textures parameters. Then the same procedure is made for shaft's eccentricity.

3.2 Surface texturing effect on viscous shear force

Figure 3 shows main and interaction effects graphs considering F_S as the analyzed journal bearing parameter. The analyses of the computational results were made using Design of Experiments (DOE) statistical methodology in accordance with Montgomery (2012). Herein low eccentricity is referred to simulations performed with $W = 1350N$ while $W = 6600N$ is associated to high eccentricity.

Apparently there is an opportunity to reduce energy dissipation inside journal bearing through full texturing when the wedge effect on the component is not pronounced as showed in Fig. 3(a). However, in high eccentricity condition the result is opposite and full texturing is not desired. That's because on last case the viscous shear force probably is more influenced by the load-carrying capacity loss than by film thickness increasing due to textures insertion. When partially texturing the bearing would be ideal to always use textures with greater radius, but the choice for deeper ones is more adequate for low eccentricity condition while in high eccentricity shallow textures are more adequate. However, diminishing in power loss is almost 2.5% for the first case. Figure 3(f) shows the catastrophic consequences of an inadequate choice of texturing parameters once the power loss in journal bearings could increase up to 10%. That's a far greater value than the best improvement made by texturing the component.

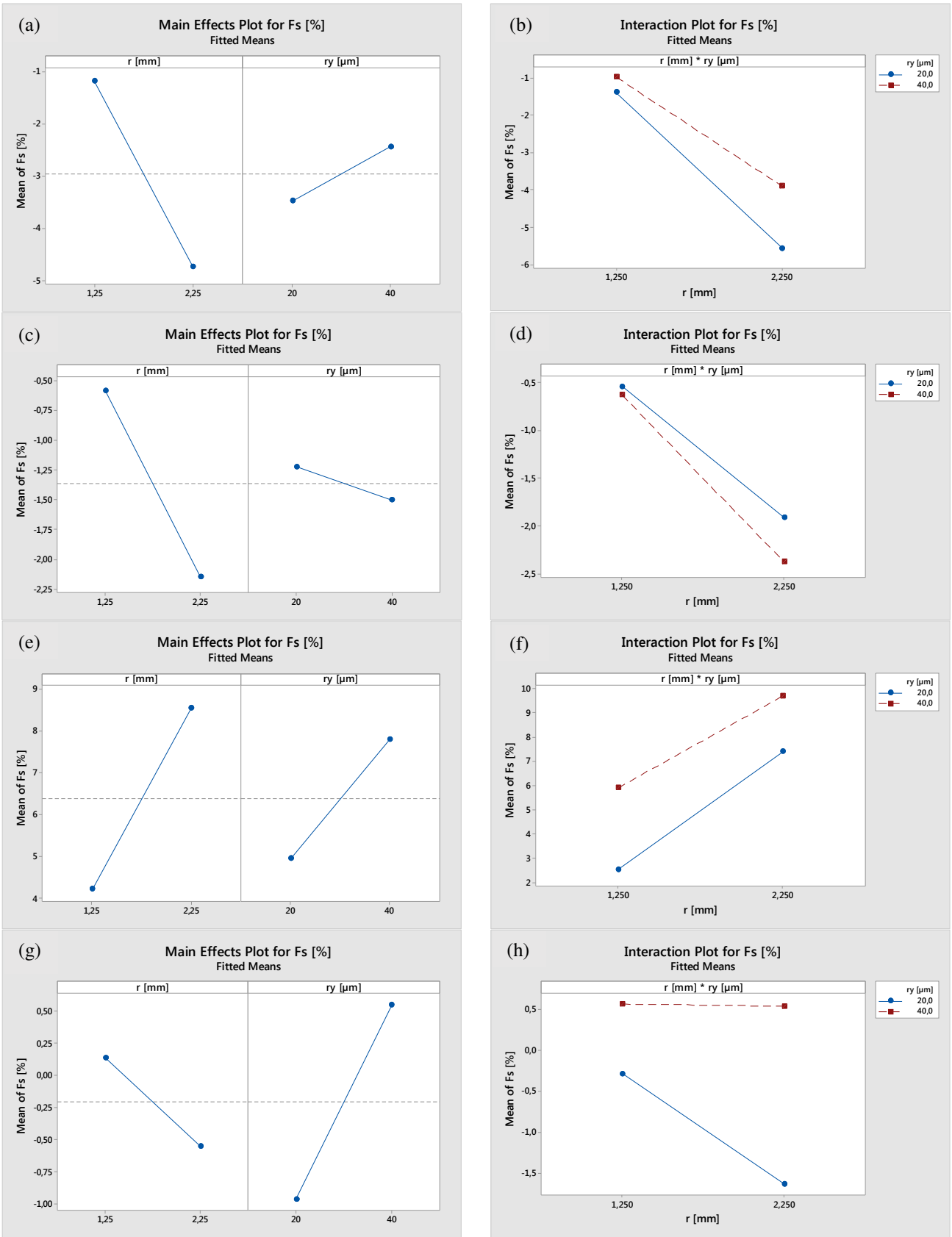

Figure 3. Main effects graphs: (a) full texturing on low eccentricity; (c) partial texturing on low eccentricity; (e) full texturing on high eccentricity; (g) partial texturing on high eccentricity. Interaction effects graphs: (b) full texturing on low eccentricity; (d) partial texturing on low eccentricity; (f) full texturing on high eccentricity; (h) partial texturing on high eccentricity.

Figure 4 shows the pressure fields for best cases in full and partial texturing of the journal bearing, both obtained for low eccentricity conditions. The power loss reduction was the observed response for that choice.

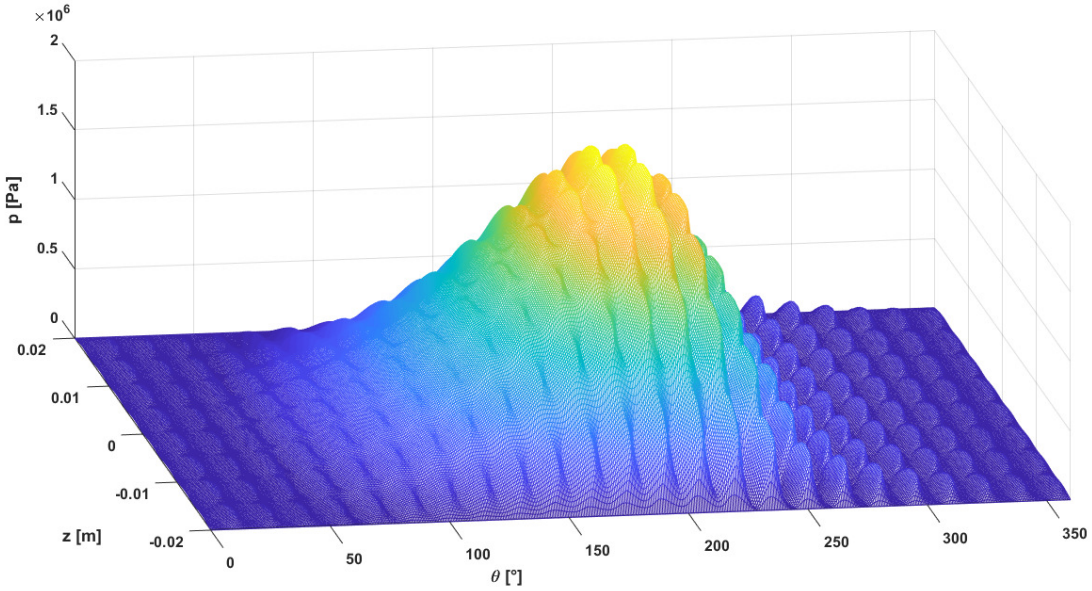

(a)

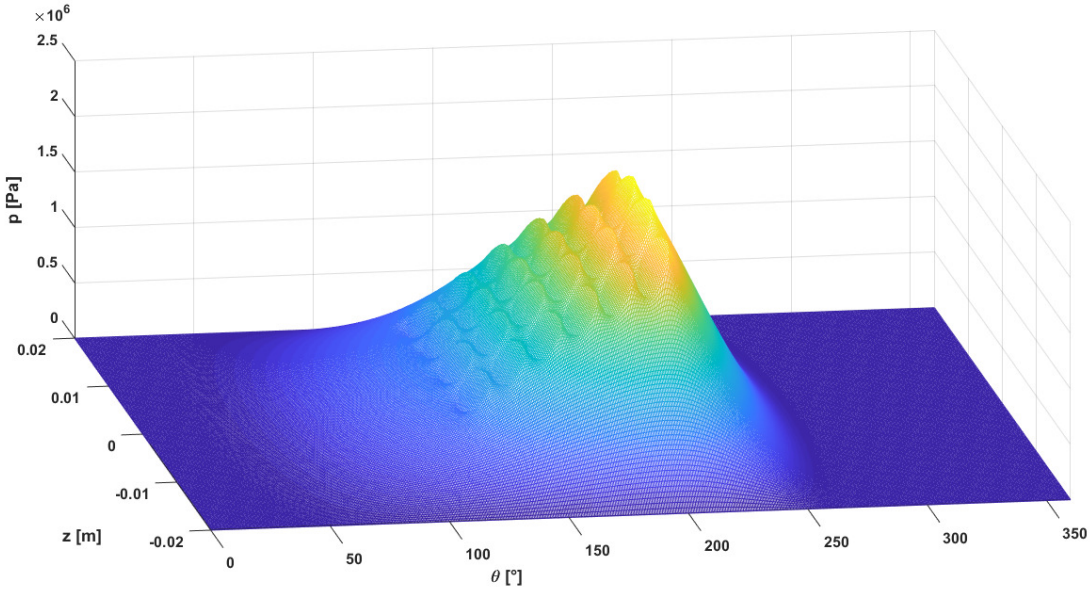

(b)

Figure 4. Pressure field for best cases of textured journal bearing: (a) full texturing; (b) partial texturing.

3.3 Surface texturing effect on load-carrying capacity

Figure 5 shows main and interaction effects graphs considering ε as the analyzed journal bearing parameter.

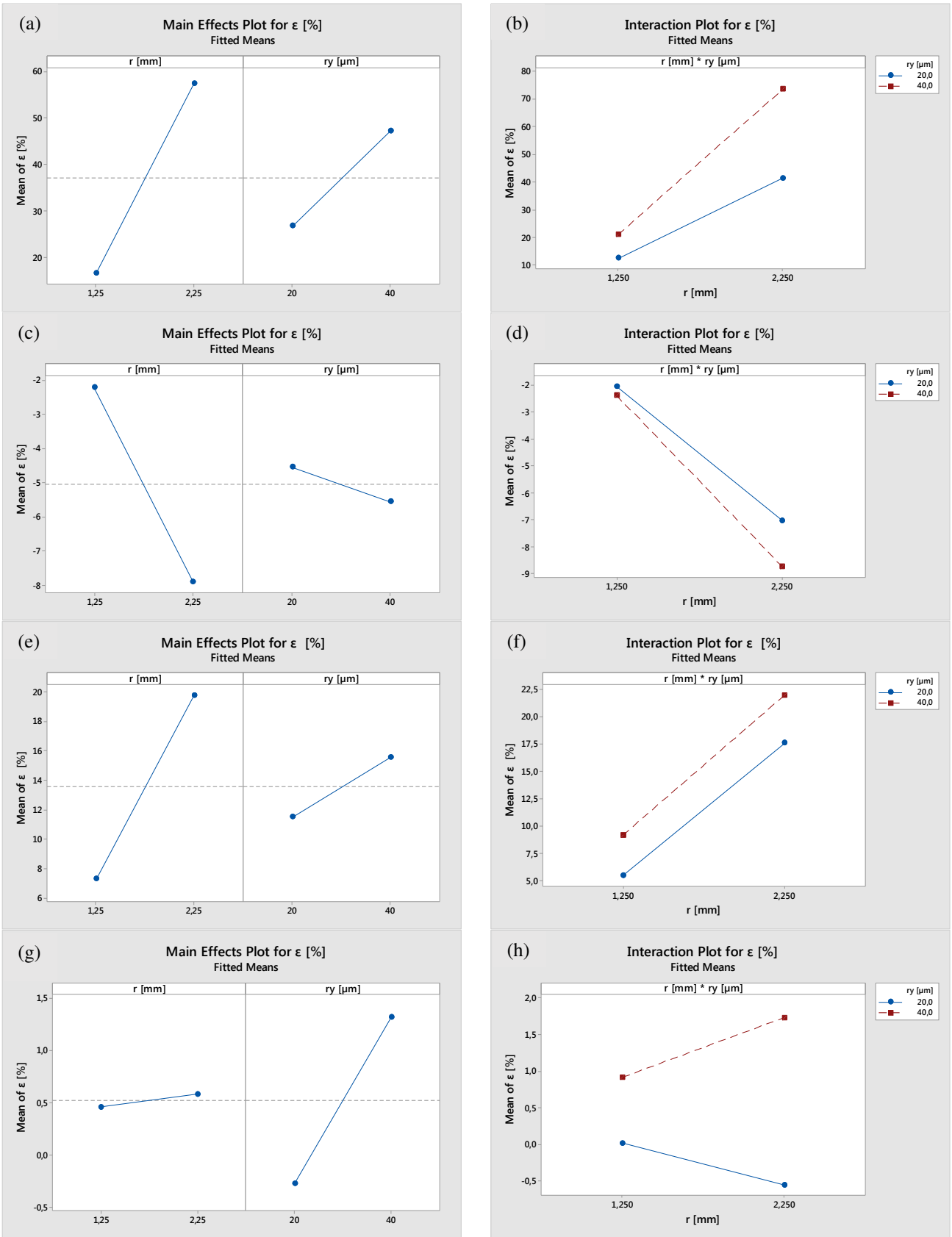

Figure 5. Main effects graphs: (a) full texturing on low eccentricity; (c) partial texturing on low eccentricity; (e) full texturing on high eccentricity; (g) partial texturing on high eccentricity. Interaction effects graphs: (b) full texturing on low eccentricity; (d) partial texturing on low eccentricity; (f) full texturing on high eccentricity; (h) partial texturing on high eccentricity.

In both full texturing cases the load capacity loss occur and a more expressive textures presence, i.e. greater radius and maximum local depth, would only prejudices the journal bearings. However it can be seen in Fig. 5(e) that a more pronounced wedge effect inside the bearing diminishes textures effects. Regarding partial texturing, operating conditions once again play a major role in changing the behavior of the analyzed factors over the eccentricity ratio. Figure 5(d) indicates that on low eccentricity conditions the choice for greater radius and depth would allow a gain in lifting of approximately 9% .On the other hand, high eccentricity condition on the bearing offers only an opportunity for a neglected change on load-carrying capacity as showed in Fig. 5(h). From Figs. 5(c) and 5(g) becomes very clear the inversion of the response's behavior with the analyzed factors, only by modifying operating conditions.

4. CONCLUSIONS

From the present study becomes clear that is possible to improve power loss when texturing journal bearings and that the best opportunities for such optimization occur although when not so prominent wedge effects are present, i.e. low eccentricity conditions. Operating conditions appear to have great influence on best textures parameters, in this study radius and major local depth, as showed for the partial texturing cases. Moreover, an erroneous textures parameters choice has a significant potential to worsen a journal bearings static characteristics and, therefore, an extensive study must be done to guarantee a correct texturing on journal bearings. Texturing of journal bearing is a defying task since modifications on pressure field are non-linear making it difficult to predict precisely the behavior of the textured component.

5. ACKNOWLEDGEMENTS

The authors would like to acknowledge CAPES and the grants 2015/20036-5 and 2015/20363-6, São Paulo Research Foundation (FAPESP).

6. REFERENCES

Etsion, I., 2013. "Modeling of surface texturing in hydrodynamic lubrication". *Friction*, Vol. 1, p. 195-209.

Gropper, D., Wang, L. and Harvey, T.J., 2016. "Hydrodynamic lubrication of textured surfaces: A review of modeling techniques and key findings". *Tribology International*, Vol. 94, p. 509-529.

Kango, S., Sharma, R.K., Pandey, R.K., 2014. "Thermal analysis of microtextured journal bearing using non-Newtonian rheology of lubricant and JFO boundary conditions". *Tribology International*, Vol. 69, p. 19-29.

Montgomery, D.C., 2001. "Design and analysis of experiments". 5th edition. New York, USA: John Wiley and Sons, Inc.

Tala-Ighil, N., Fillon, M., Maspeyrot, P., 2011. "Effect of textured area on the performances of a hydrodynamic journal bearing". *Tribology International,* Vol 44, p. 211-219.

Venner, C.H. and Lubrecht, A.A., 2000. "Multilevel methods in lubrication". Netherlands: Elsevier, Tribology Series, v.37, 400p.

Wang, L., 2014. "Use of structured surfaces for friction and wear control on bearing surfaces". *Surf. Topogr.: Metrol. Prop.*, Vol. 2, p. 043001.

7. RESPONSIBILITY NOTICE

The authors are the only responsible for the printed material included in this paper.